

Evolution of helium white dwarfs with hydrogen envelopes

O. G. Benvenuto^{★†} and L. G. Althaus^{★‡}

Facultad de Ciencias Astronómicas y Geofísicas, Universidad Nacional de La Plata, Paseo del Bosque S/N, (1900) La Plata, Argentina

Accepted 1997 September 1. Received 1997 September 1; in original form 1997 April 2

ABSTRACT

The present study is aimed at exploring the effects of hydrogen envelopes on the structure and evolution of low- and intermediate-mass, helium white dwarfs. To this end, we compute the evolution of models of helium white dwarfs with masses ranging from 0.15 to 0.5 M_{\odot} for low and intermediate effective temperatures. We treat the mass of the hydrogen envelope as a free parameter within the range $10^{-8} \leq M_{\text{H}}/M \leq 4 \times 10^{-3}$. The calculations are carried out by means of a detailed white dwarf evolutionary code in which updated radiative opacities and equations of state for hydrogen and helium plasmas are considered. The energy transport by convection is described by the full spectrum turbulence theory developed by Canuto, Goldman & Mazzitelli, which has no free parameters. We also take into account both convective mixing in the outer layers occurring at low luminosities and the presence of hydrogen burning at the bottom of the hydrogen-rich envelope by means of the inclusion of a detailed network of thermonuclear reaction rates.

Our attention is focused mainly on that phase of evolution where finite-temperature effects are particularly significant. In this respect, we find that thick hydrogen envelopes appreciably modify the radii and surface gravity of the no-hydrogen models, especially in the case of low-mass configurations. In addition, convective mixing in low-luminosity models with thin hydrogen envelopes leads to objects with helium-dominated outer layers. Finally, we find that the role played by hydrogen burning in these stars is strongly dependent on the mass of the hydrogen envelope.

The computations presented here represent the most detailed models of helium white dwarfs with hydrogen envelopes presently available. These models should be particularly valuable for the study of the structure and evolutionary status of the recently detected low-mass white dwarfs in binary systems.

Key words: stars: evolution – stars: interiors – pulsars: general – white dwarfs.

1 INTRODUCTION

Helium white dwarf (He WD) stars have recently begun to be detected in various binary configurations. Evidence gathered over recent years confirms the idea that He WDs

would be the result of the evolution of close binary systems. Indeed, Marsh (1995), Marsh, Dhillon & Duck (1995), Marsh & Duck (1996), Lundgren et al. (1996) and Moran, Marsh & Bragaglia (1997), among others, detected low-mass WDs in binary systems containing another WD or a millisecond pulsar. Furthermore, a very low-mass WD in a binary system containing a yellow giant has been recently reported by Landsman et al. (1997). More precisely, on the basis of ultraviolet observations these authors conclude that the yellow giant S1040 in the open cluster M67 belongs to a binary system in which the secondary is an He WD with a mass as low as 0.22 M_{\odot} . In addition, numerical models of close binary degenerate dwarfs (Iben, Tutukov & Yungel-

[★]E-mail: obenvenuto@fcaglp.fcaglp.unlp.edu.ar (OGB);
althaus@fcaglp.fcaglp.unlp.edu.ar (LGA)

[†]Member of the Carrera del Investigador Científico, Comisión de Investigaciones Científicas de la Provincia de Buenos Aires (CIC), Argentina.

[‡]Fellow of the Consejo Nacional de Investigaciones Científicas y Técnicas (CONICET), Argentina.

son 1996) indicate that in the majority of the systems consisting of two close WDs, the brighter component is expected to be an He WD. Such stars would ensue from the evolution of some binary systems as long as the first Roche lobe overflow phase takes place prior to He burning in the primary star (see Iben & Livio 1993 and references therein for details).

Needless to say, an adequate interpretation of all these observational data requires models of He WDs based on a physical description as accurate and as detailed as possible. In a previous paper (Althaus & Benvenuto 1997a, hereafter Paper I), we computed the structure and evolution of low- and intermediate-mass He WD models without a hydrogen (H) envelope (such models will be hereafter referred to as no-H models) by taking fully into account finite-temperature effects. In that work we included a very detailed physical description, such as the recently available equations of state for He plasmas and OPAL radiative opacities. One of the most relevant features of that study is that the energy transport by convection is described by the full spectrum turbulence theory (Canuto & Mazzitelli 1991, 1992; hereafter CM), which has been shown to provide a good description of convection in WD stars with He-dominated outer layers (see Althaus & Benvenuto 1996). The calculations presented in Paper I constitute the most extensive study of low-mass He WDs without H to date, and the evolution of central conditions, radii, surface gravities, neutrino luminosity and ages of models were carefully examined.

It is worth emphasizing that sufficiently detailed models of low-mass WDs should be very valuable in shedding new light on multiple aspects of the study of millisecond pulsars. The observations carried out recently by van Kerkwijk, Bergeron & Kulkarni (1996) are particularly noteworthy in this regard. These authors managed to bracket the mass of the pulsar J1012 + 5307 as being between 1.5 and 3.2 M_{\odot} from spectroscopic data inferred from its low-mass, DA WD companion combined with a very simplified theoretical mass–radius relation for the WD. A more precise determination of the pulsar mass may reveal important clues about, for instance, the equation of state at the ultrahigh densities attained at neutron star interiors. As claimed by van Kerkwijk et al., detailed low-mass WD models with H envelopes are required in order to improve our knowledge about this relevant issue.

In view of these considerations, we extend in this paper the calculations presented in Paper I to the case of low- and intermediate-mass He WD models with H envelopes, with the aim of analysing the effect of such envelopes on the structure and cooling of these stars. Unfortunately, since the amount of H material remaining above the He core after the common-envelope phase remains a poorly constrained parameter by stellar evolution theory, one is forced to treat this quantity basically as a free parameter (see Iben & Livio 1993 for a detailed discussion of the common-envelope phase).

In this study, we carry out some modifications to the constitutive physics of the models presented in Paper I, notably the theory of convection. As a matter of fact, we now describe the energy transport by convection according to the self-consistent model for stellar turbulence convection recently developed by Canuto, Goldman & Mazzitelli

(1996, hereafter CGM). This new model, like the CM one, is based on the full spectrum turbulence theory and does not have parameters that must be calibrated. However, it considers a self-consistent rate of energy input; that is, the energy input from the source (buoyancy) into the turbulence depends now on both the source and the turbulence itself. This feature represents an improvement with respect to the CM model and makes the CGM model self-consistent. In particular, at low and intermediate convective efficiencies, the CGM model provides higher convective fluxes than does the CM one. In the case of our Sun, CGM found that their new model predicts a better agreement with recent observational data than the CM model. On the basis of detailed evolutionary calculations, Althaus & Benvenuto (1997b) (see also Benvenuto & Althaus 1997) have shown that, in the WD domain, the CGM model yields an excellent agreement with recent observations of the pulsating DB WD GD 358, reported by Provencal et al. (1996).

In this study, we compute He WD models with masses ranging from 0.15 to 0.5 M_{\odot} , with steps of 0.05 M_{\odot} for low and intermediate effective temperatures (T_{eff}). To assess the sensitivity of our results to the mass of an outer H layer, we vary the mass of such an envelope in the interval of $10^{-8} \leq M_{\text{H}}/M \leq 4 \times 10^{-3}$, where M_{H} and M are the H envelope and model masses, respectively. Also, for the sake of a consistent comparison, we also calculate the evolution of no-H models. The calculations are carried out by means of a full stellar evolutionary code developed by us in which we include the most recently available input physics. Chiefly, OPAL radiative opacities (Rogers & Iglesias 1994), molecular opacities (Alexander & Ferguson 1994), the equation of state for He and H composition developed by Saumon, Chabrier & Van Horn (1995) and, as mentioned, the CGM model are considered. We also include neutrino energy losses as well as convective mixing in the outer layers of the models. Finally, we incorporate in our WD evolutionary code the complete network of thermonuclear reaction rates for H burning (proton–proton chain and CNO bi-cycle). The change in the chemical composition (a total of 16 chemical elements are included) are computed by means of an implicit method of integration.

In this work, we focus the discussion mainly on those evolutionary stages where finite-temperature effects are significant. In this respect, we shall show that thick H envelopes appreciably modify the surface gravity of the no-H models, especially in the case of low-mass configurations. In addition, we shall see that, depending on the mass of the H envelope, convective mixing operating in low-luminosity models may change drastically the surface composition of He WDs. Also, we shall discuss the role played by H burning in these stars, particularly in the context of evolutionary times. Finally, we shall see that whether H burning is an important source of stellar energy or not strongly depends upon the H envelope mass, a result also found by Koester & Schönberner (1986) in the context of carbon–oxygen WDs (see also D’Antona & Mazzitelli 1979).

The set of models of He WDs with H envelopes presented here is the most detailed set presently available. Thus, they should be particularly valuable as a reference for the study of the general characteristics of such objects and even to infer information from the companion object in binary systems.

The remainder of this paper is organized as follows. In Section 2, we comment on our WD evolutionary code and the main physical ingredients we included in this study, in particular the CGM model; Section 3 is devoted to presenting and analysing our results and, finally, in Section 4 we summarize our findings.

2 COMPUTATIONAL DETAILS

2.1 Evolutionary code and initial models

The calculations were carried out with the same evolutionary code we employed in our previous works on WD evolution. The code is fully described in Benvenuto & Althaus (1995), Paper I and Benvenuto & Althaus (1997).

The procedure we employed to obtain the initial models is also detailed in Paper I and we shall not repeat it here, except regarding the way in which an H envelope is added. Such an envelope was included by means of an artificial evolutionary procedure, in which we changed the chemical composition of a given (previously selected) outermost fraction of the model from He to H in about 20 successive models. In order to obtain the appropriate initial model, we neglected the effect of H burning on the chemical composition but not the nuclear energy release (although it is very small before the relaxation of the isotopic abundances occurs). We regard to the initial chemical abundances assumed in the just-‘created’ H layer, we considered it to be made up only of ^1H , ^{12}C and ^{16}O , assuming for each of the last two species an abundance by mass of 5×10^{-4} . After such artificial evolution, the model undergoes a transitory relaxation to a physically plausible structure in about 40 models. In this work we considered as meaningful those models computed after such relaxation.

In contrast to Paper I, all of the calculations presented here were started from initial models resembling WD structures. We stress that the early evolution of our models is affected by our choice of the initial model; accordingly, all of our models should be considered as evolutionary phases that may be reached asymptotically as a product of evolution of binary systems (see Paper I for details).

Because the mass of the H envelope able to survive the common-envelope event is only weakly constrained by theory, we have decided to treat this quantity as essentially a free parameter within the range $10^{-8} \leq M_{\text{H}}/M \leq 4 \times 10^{-3}$. Finally, the H/He transition zone was assumed to be rather discontinuous and convective mixing was fully taken into account.

2.2 Equation of state, opacities, hydrogen burning and convection

A description of the different equations of state employed in this study can be found in Paper I. In particular, for the low-density regime, we follow the treatment presented by Saumon et al. (1995) for H and He plasmas, which offers a detailed description of the thermodynamic state of matter under the conditions found in cool, dense objects such as WD envelopes, giant planets and low-mass stars. This equation of state, in particular that corresponding to the H plasma, is quite detailed and remains the most extensive treatment available at present (at least at the cold and dense conditions for which it was computed). The equation of

state we use to describe the completely ionized, degenerate plasma appropriate for the deep interior of WDs was developed by us and is described in Paper I.

With regard to opacities, for the high-temperature regime ($T \geq 8000$ K) we use OPAL radiative opacities (Iglesias & Rogers 1993) with metallicity $Z=0.001$. For lower temperatures and depending on the H content, these tables are complemented either with the Alexander & Ferguson (1994) molecular opacities or (if $X_{\text{H}} < 0.10$, where X_{H} is the H abundance fraction by mass) with the Cox & Stewart (1970) data.¹ Alexander & Ferguson computed Rosseland mean opacities for temperatures between 12 500 and 700 K and found that, at temperatures as high as 5000 K and high densities, molecules begin to play a significant role and that for temperatures below 2500 K they become the dominant source of opacity. Conductive opacities and the various mechanisms of neutrino emission appropriate for WD interiors are taken from the works of Itoh and collaborators, and we refer the reader to Paper I for details. It is worth mentioning that, except for models at low luminosities, the set of opacities cited above covers most of the conditions characterizing the interior of our evolving models.

For models with sufficiently thick H envelopes, H burning is not negligible, thus reducing the mass of the H envelope substantially. To compute this effect we include in our WD evolutionary code the complete network of thermonuclear reaction rates for H burning corresponding to the proton–proton chain and the CNO bi-cycle. Specifically, we compute the abundances of the following chemical species: ^1H , ^2H , ^3He , ^4He , ^7Li , ^7Be , ^8B , ^{12}C , ^{13}C , ^{13}N , ^{14}N , ^{15}N , ^{15}O , ^{16}O , ^{17}O and ^{17}F . Nuclear reaction rates are taken from Caughlan & Fowler (1988), whereas β -decay rates are taken from Wagoner (1969), taking into account the corrections for their Q -values due to neutrino losses. Electron screening is taken from Wallace, Woosley & Weaver (1982).

The changes in the chemical composition are evaluated by means of a standard implicit method of integration in which the effects of abundance changes of other species on the change of a given species are taken into account via a matrix equation (see Arnett & Truran 1969 for details).

Finally, as we mentioned earlier, the energy transport by convection is described by the self-consistent model for turbulent convection recently developed by CGM. They considered the full spectrum of eddies as contributing to the convective flux, and fitted their theoretical results for the convective flux F_c with the expression

$$F_c = KTH_p^{-1}(\nabla - \nabla_{\text{ad}})\Phi, \quad (1)$$

where $K = 4acT^3/3k\rho$ is the radiative conductivity, H_p is the pressure scaleheight and ∇ and ∇_{ad} are, respectively, the true and adiabatic temperature gradients. Φ is given by

$$\Phi = F_1(S)F_2(S), \quad (2)$$

where

$$F_1(S) = \left(\frac{K_0}{1.5}\right)^3 aS^k [(1 + bS)^l - 1]^q. \quad (3)$$

¹ We stress that this rather old opacity tabulation remains the only one available and the only one compatible with OPAL data for He-dominated plasmas for the conditions relevant here. For more details, see Paper I.

Here, K_0 is the Kolmogorov constant (assumed to be 1.8), $S=162A^2(\nabla-\nabla_{\text{ad}})$ and the coefficients are given by $a=10.8654$, $b=4.89073 \times 10^{-3}$, $k=0.149888$, $l=0.189238$ and $q=1.85011$. A is given in Benvenuto & Althaus (1997; see their equation 6), and

$$F_2(S) = 1 + \frac{cS^{0.72}}{1+dS^{0.92}} + \frac{eS^{1.2}}{1+fS^{1.5}}, \quad (4)$$

where $c=1.08071 \times 10^{-2}$, $d=3.01208 \times 10^{-3}$, $e=3.34441 \times 10^{-4}$ and $f=1.25 \times 10^{-4}$.

Among the advantages of the CGM model (and the CM one) is that it contains no parameters that must be calibrated. In particular, the mixing length is taken to be the geometrical distance from the top of the convection zone to the point where ∇ is computed.

It is important to note that in the present paper we have neglected the effects of diffusion on the evolution of the models. Such effects should be of some importance in the exact rate of H burning and the age of the models, especially in the most massive cases. However, we expect the radius (and thus the gravitational acceleration g) of the models to be fairly insensitive to such physical process. For a study of the effects of diffusion on the evolution of carbon–oxygen WDs with H envelopes, see Iben & McDonald (1985).

3 EVOLUTIONARY RESULTS

We present now the main results of our calculations. We computed the evolution of models with masses ranging from $M=0.15$ to $0.5 M_{\odot}$ at intervals of $0.05 M_{\odot}$ and with a metallicity of $Z=0.001$. We varied M_{H} within the range $10^{-8} \leq M_{\text{H}}/M \leq 4 \times 10^{-3}$. More specifically, for the 0.5- and 0.45- M_{\odot} models we used H envelopes with $M_{\text{H}}/M=0, 10^{-8}, 10^{-6}, 10^{-4}, 2 \times 10^{-4}, 4 \times 10^{-4}$; for the 0.4- and 0.35- M_{\odot}

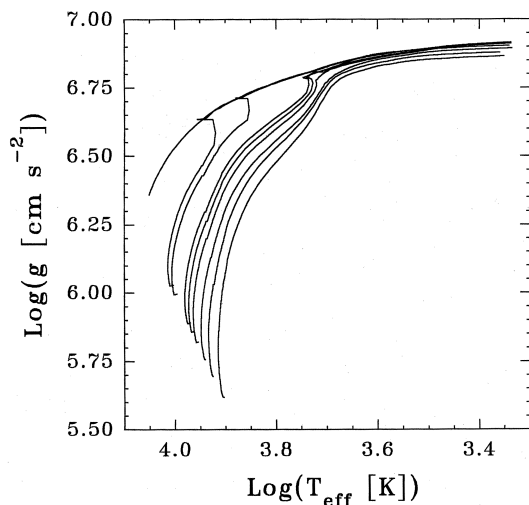


Figure 1. Surface gravities versus T_{eff} for 0.15- M_{\odot} He WD models with different H envelopes. At high T_{eff} and from top to bottom, the curves correspond to sequences with $M_{\text{H}}/M=0, 10^{-8}, 10^{-6}, 10^{-4}, 2 \times 10^{-4}, 4 \times 10^{-4}, 1 \times 10^{-3}, 2 \times 10^{-3}$ and 4×10^{-3} . Note that thick H envelopes appreciably modify the g values of the no-H model, especially at high T_{eff} values. Note also that at a given T_{eff} , g values of models with very thin H envelopes becomes identical to that of the no-H model as a result of convective mixing.

models we also included $M_{\text{H}}/M=10^{-3}$; for the 0.3- and 0.25- M_{\odot} models we used the same envelopes as for the 0.35- M_{\odot} model and $M_{\text{H}}/M=2 \times 10^{-3}$ as well. Finally, for the 0.20- and 0.15- M_{\odot} models we also considered the case $M_{\text{H}}/M=4 \times 10^{-3}$. These models were evolved from the hot WD stage down to $\log(L/L_{\odot})=-5$. With these calculations we extend those presented in Paper I to the case of low-mass WD models with H envelopes. Here, we are mainly concerned with the effects of varying the mass of the H envelope on the structure and cooling of He WD models.

We begin by examining Figs 1–8 in which the surface gravity g as a function of T_{eff} is shown for He WD models with $M/M_{\odot}=0.15, 0.20, 0.25, 0.30, 0.35, 0.40, 0.45$ and 0.50 and the corresponding values of M_{H} mentioned in the foregoing paragraph. The first observation we can make from these figures is that thick H envelopes appreciably modify the g value of no-H models, especially in the case of low-mass configurations. At $T_{\text{eff}} \approx 17000$ K for instance, the g

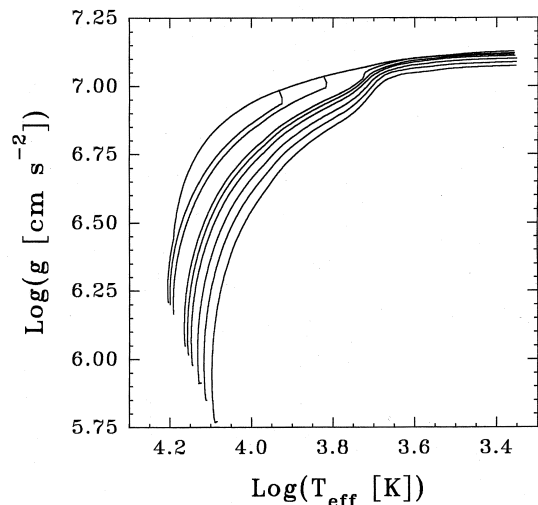


Figure 2. Same as Fig. 1 but for 0.20- M_{\odot} He WD models.

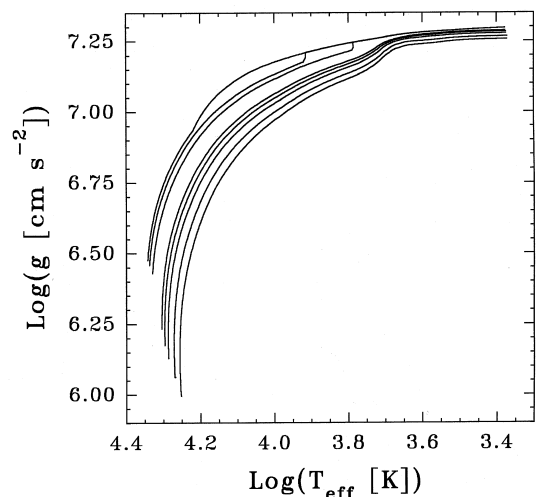
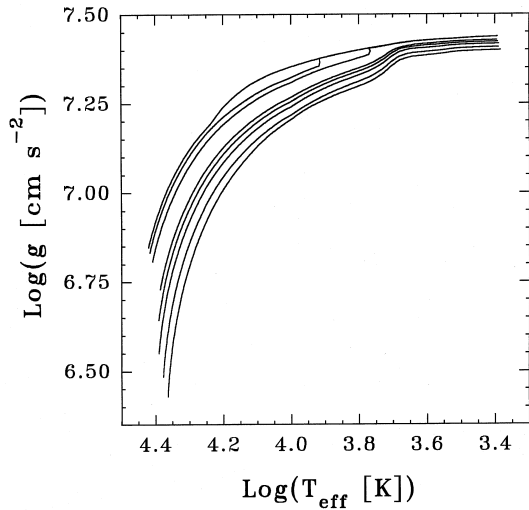
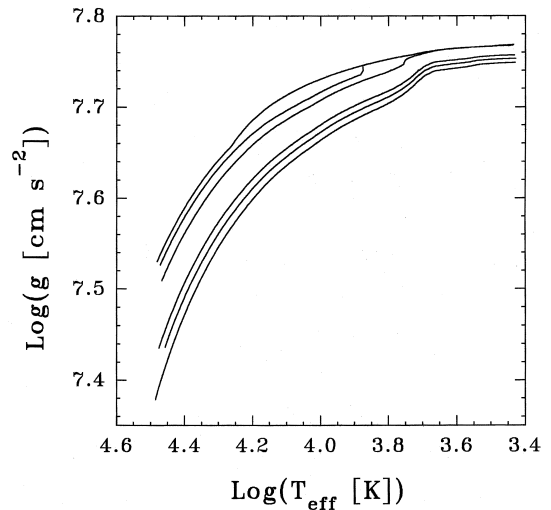
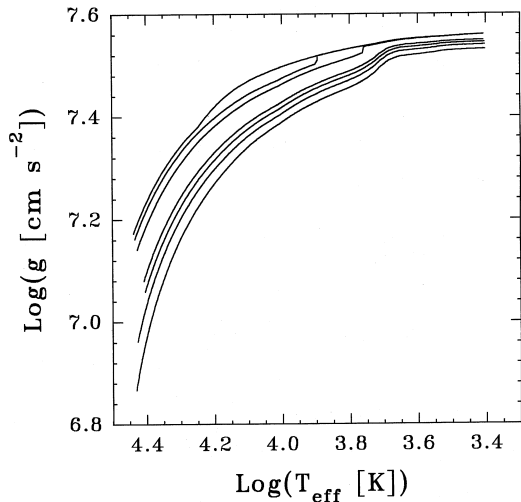
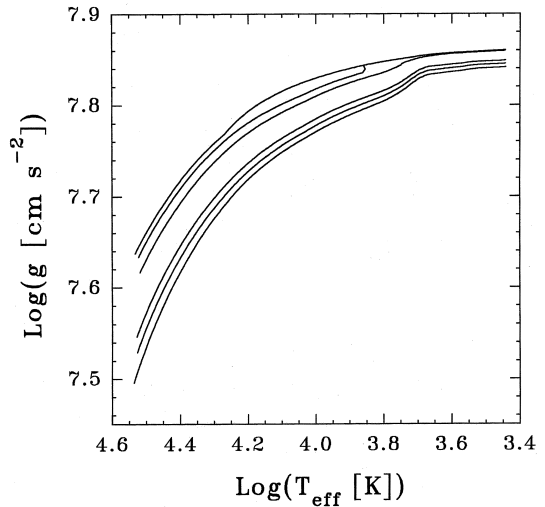
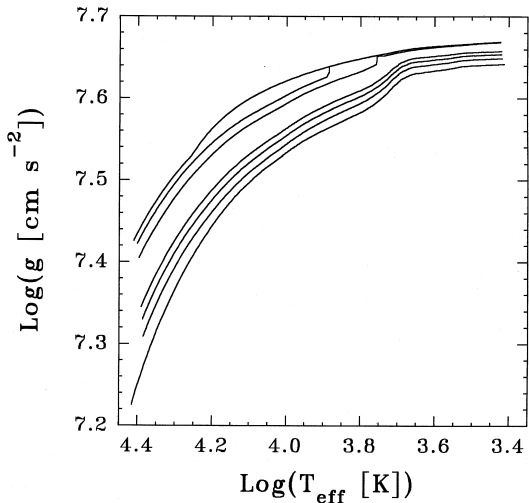


Figure 3. Same as Fig. 1 but for 0.25- M_{\odot} He WD models. Now, we depict models with M_{H} values up to $M_{\text{H}}/M=2 \times 10^{-3}$.


 Figure 4. Same as Fig. 3 but for 0.30- M_{\odot} He WD models.

 Figure 7. Same as Fig. 1 but for 0.45- M_{\odot} He WD models. Now, we depict models with M_{H} values up to $M_{\text{H}}/M=4 \times 10^{-4}$.

 Figure 5. Same as Fig. 1 but for 0.35- M_{\odot} He WD models. Now, we depict models with M_{H} values up to $M_{\text{H}}/M=10^{-3}$.

 Figure 8. Same as Fig. 7 but for 0.50- M_{\odot} He WD models.

 Figure 6. Same as Fig. 5 but for 0.40- M_{\odot} He WD models.

value of the 0.25- M_{\odot} , no-H model is approximately 80 per cent larger than the surface gravity of the model with the same stellar mass but with an H envelope of $M_{\text{H}}/M=4 \times 10^{-4}$. Another feature worthy of comment exhibited by these figures is the fact that at a given T_{eff} the surface gravity of models with very thin H envelopes becomes identical to that of no-H models. In fact, the penetration of the H convection zone into the underlying He interior causes the surface X_{H} (hereafter $X_{\text{H}}^{\text{sur}}$) in models with very thin H layers to drop markedly (by several orders of magnitude in some cases: see later in this section). This process leads to objects with He-dominated outer layers. From then on, their subsequent evolution strongly resembles that of an He WD model with a no-H envelope. Note that at $T_{\text{eff}} \approx 5000$ K the curves corresponding to models with thick H envelopes tend to approach the curves for no-H models. This behaviour is attributed to the fact that the atmospheric and subatmospheric layers of such models become substantially

more transparent to radiation as a result of the strong decrease in opacity as the temperature goes below that corresponding to the onset of H ionization. This leads to denser outer layers and thus to models with appreciably smaller (larger) radius (g).

For the sake of a rigorous comparison between the various models, we depict in Fig. 9 the values of g versus T_{eff} for the full set of sequences computed in this investigation. Both the finite-temperature effects even in massive models and, more importantly, the magnitude of the changes in g brought about by rather thick H envelopes are apparent. In this respect, we note, for example, that, in the hot stage of evolution, the g values corresponding to a sequence of a given mass with the thickest H envelope considered takes after approximately the surface gravity corresponding to a pure-He model but with a mass $0.05 M_{\odot}$ lower. This is a very important point to be made if we want to measure the mass of low-mass WDs by means of the g - T_{eff} relationship, and, so, this procedure should be carefully carried out in order to estimate the actual inherent uncertainties (largely due to the impossibility of measuring M_{H} for each object).

In Figs 10–12 we show the Hertzsprung–Russell diagram for 0.15-, 0.20- and 0.30- M_{\odot} He WD models with different H envelopes. At low luminosities, the evolutionary tracks follow lines of constant radius, as expected for strongly degenerate configurations. It is worth noting that models with thicker H envelopes are characterized by less dense outer layers and, accordingly, they have lower T_{eff} (larger radius) at a given luminosity. Note also the effect of convective mixing on low-mass models with very thin H envelopes, which gives rise to a transient increase in the surface luminosity. Afterwards, their evolutionary tracks resemble those of no-H models.

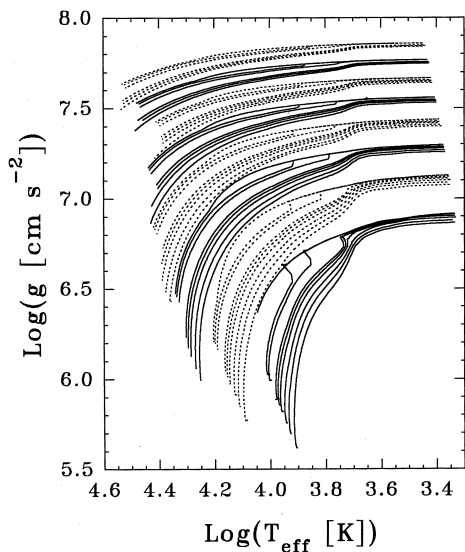


Figure 9. Surface gravity versus T_{eff} relation for He WD models with (from top to bottom) $M/M_{\odot}=0.5, 0.45, 0.4, 0.35, 0.3, 0.25, 0.20$ and 0.15 in an alternate sequence of short-dashed and solid lines. For each stellar mass, we show all the values included in Figs 1–8. The changes in g brought about by the different H envelopes are more noticeable at high T_{eff} , particularly for less massive models. Note also that finite-temperature effects are very important even in rather massive models.

In order to further clarify the effect of the convective mixing on the outer layer composition, we plot in Fig. 13 the evolution of $X_{\text{H}}^{\text{sur}}$ in terms of T_{eff} for 0.20-, 0.30-, 0.40- and 0.50- M_{\odot} He WD models. This point deserves some words of caution. It is well known that the size of the outer convective zone in WDs is strongly dependent on the description assumed for the convective transport. Consequently, the values of T_{eff} at which mixing occurs are also dependent on the particular formulation of convection. The CGM model we employ in this study has been shown to work very well in describing convection in the outer layers of DB WDs (Althaus & Benvenuto 1997b). A recent study (Althaus & Benvenuto 1997c) seems to point out that CGM model does not fit the observations of DA WDs so well as in the DB case. Because of this fact, our T_{eff} values at which mixing occurs should not be taken as a definitive one. In any case,

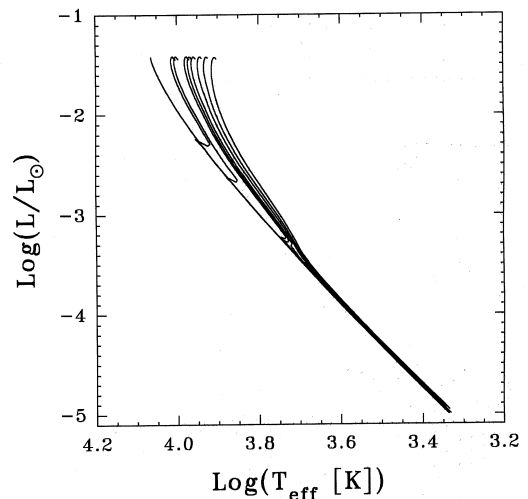


Figure 10. Theoretical Hertzsprung–Russell diagram for 0.15- M_{\odot} He WD models with the different H envelopes detailed in Fig. 1. As expected, models with thicker H envelopes are characterized by lower T_{eff} at a given luminosity. Note also the effect of convective mixing on models with very thin H envelopes.

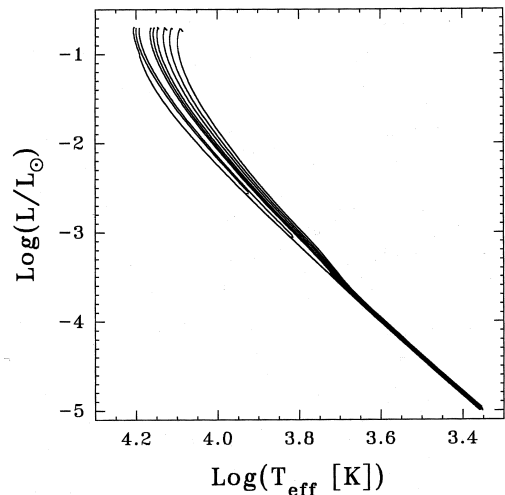


Figure 11. Same as Fig. 10 but for 0.20- M_{\odot} He WD models.

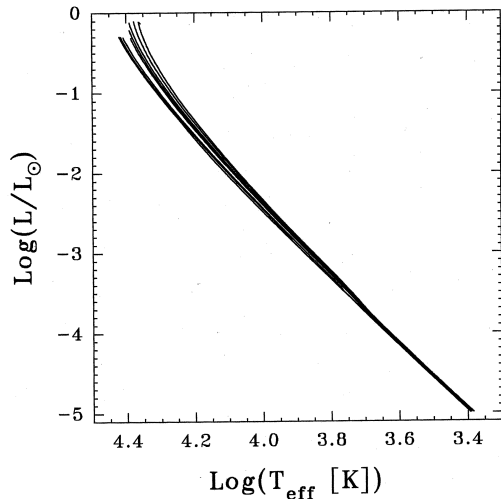


Figure 12. Same as Fig. 11 but for 0.30- M_{\odot} He WD models. The M_{H} values included in this figure are specified in Fig. 4.

we think that CGM remains the most trustworthy model of stellar convection available at present.

It is clear from Fig. 13 that the surface composition of models with very thin H envelopes changes drastically from an H-dominated to an He-dominated one as a result of convective mixing occurring at low T_{fr} . By contrast, $X_{\text{H}}^{\text{sur}}$ in models with very thick H envelopes remains constant throughout the entire evolution or consists of a mixture of H and He in the case of H envelopes with intermediate thickness. This behaviour is, of course, related to the fact that the base of the convection zone in the evolving models ultima-

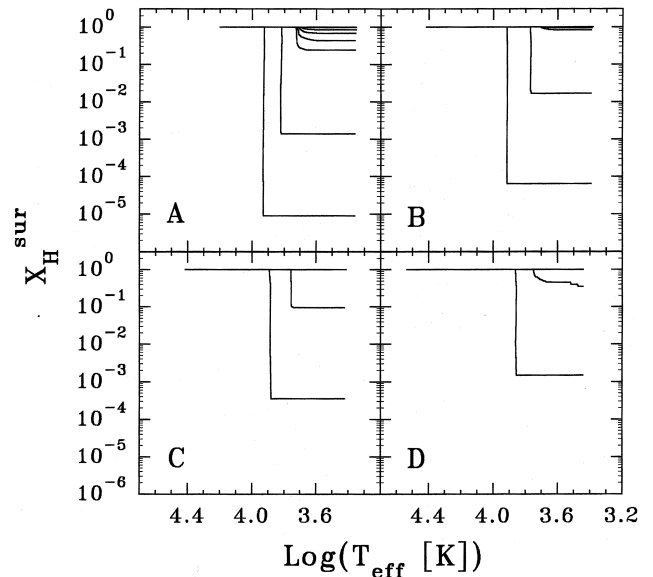


Figure 13. Evolution of $X_{\text{H}}^{\text{sur}}$ in terms of T_{eff} for the same stellar masses and H envelopes as in Fig. 14 (the smaller M_{H} , the smaller the final $X_{\text{H}}^{\text{sur}}$). In panel A, from bottom to top the change in $X_{\text{H}}^{\text{sur}}$ can be distinguished for models with the six thinner H envelopes. In panel B only the three thinner can be noticed, whereas, in panels C and D only the two thinner show appreciable changes. This is because less massive models, develop larger convection zones. For more details, see Table 1.

tely reaches the domain of electron degeneracy and thus a maximum depth. For more details, we list in Table 1 the T_{eff} values at which $X_{\text{H}}^{\text{sur}}$ begins to change appreciably as a result

Table 1. Mixing temperatures and final hydrogen abundance for different models.

Sequence	T_{eff}^m (K)	$X_{\text{H}}^{\text{sur}}$	Sequence	T_{eff}^m (K)	$X_{\text{H}}^{\text{sur}}$
0.50 (1E-8)	7270	1.5E-3	0.25 (4E-4)	4960	0.90
0.50 (1E-6)	5630	0.45	0.20 (1E-8)	8410	1E-5
0.45 (1E-8)	7620	7E-4	0.20 (1E-6)	6570	1.4E-3
0.45 (1E-6)	5700	0.20	0.20 (1E-4)	5330	0.30
0.40 (1E-8)	7800	3.5E-4	0.20 (2E-4)	5270	0.50
0.40 (1E-6)	5730	0.095	0.20 (4E-4)	5160	0.75
0.35 (1E-8)	7970	1.7E-4	0.20 (1E-3)	5000	0.85
0.35 (1E-6)	5780	0.051	0.15 (1E-8)	8300	2E-6
0.30 (1E-8)	8240	6.4E-5	0.15 (1E-6)	7120	2E-4
0.30 (1E-6)	5890	0.017	0.15 (1E-4)	5430	0.067
0.30 (1E-4)	5130	0.83	0.15 (2E-4)	5370	0.1
0.30 (2E-4)	4830	0.95	0.15 (4E-4)	5250	0.2
0.25 (1E-8)	8340	3E-5	0.15 (1E-3)	5150	0.45
0.25 (1E-6)	6160	5.3E-3	0.15 (2E-3)	5080	0.75
0.25 (1E-4)	5240	0.58	0.15 (4E-3)	4960	0.85
0.25 (2E-4)	5130	0.77			

Note. Each sequence is denoted by the stellar mass (in solar mass units). The numbers in parentheses indicate the value of the initial M_{H} envelope in terms of the stellar mass.

of convective mixing. The final $X_{\text{H}}^{\text{sur}}$ after the main mixing episodes have taken place is also tabulated. Mixing is absent or it barely occurs (thus slightly modifying $X_{\text{H}}^{\text{sur}}$) for the other envelopes considered in this study and not listed in Table 1. Clearly, the mixing temperature depends upon both M_{H} and the model mass. In particular, $X_{\text{H}}^{\text{sur}}$ for our 0.20- M_{\odot} model with $M_{\text{H}}/M=10^{-8}$ (the smallest H envelope we used) does not change until the model reaches $T_{\text{eff}} \approx 8500$ K.

The H-burning luminosity as a function of surface luminosity for He WD models with $M/M_{\odot}=0.2, 0.3, 0.4$ and 0.5 and with different H envelopes is shown in Fig. 14. It is clear that the H-burning luminosity strongly depends upon M_{H} (see D’Antona & Mazzitelli 1979 for a similar result). Note also the sharp increase in the H-burning luminosity for very thin H envelope models resulting from the penetration of the H convection zone into the underlying He interior, causing some H to reach hotter layers. It is worth adding that in the case of those models that have the largest H envelopes considered in this study, H burning contributes substantially to the total luminosity throughout the range of intermediate luminosity but never becomes the dominant source of energy. More specifically, as far as the 0.5- M_{\odot} model with $M_{\text{H}}/M=4 \times 10^{-4}$ is concerned, H burning contributes more than 10 per cent to the total luminosity in the range $-3.2 \lesssim \log(L/L_{\odot}) \lesssim -1.7$ ($7500 \lesssim T_{\text{eff}} \lesssim 16\,900$ K), reaching a maximum of 25 per cent at $\log(L/L_{\odot}) = -2.6$ ($T_{\text{eff}} \approx 10\,500$ K). These quantities vary considerably with stellar mass. Indeed, the H-burning contribution to surface luminosity of the 0.45- and 0.40- M_{\odot} models with $M_{\text{H}}/M=4 \times 10^{-4}$, for instance, remains always below 11 and 4 per cent, respectively. Needless to say, lower stellar masses require larger H envelopes in order for H burning to contri-

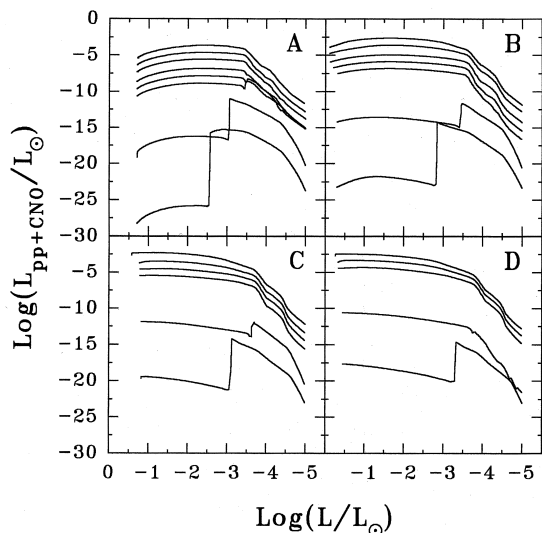


Figure 14. H-burning luminosity as a function of surface luminosity for He WD models with $M/M_{\odot}=0.2, 0.3, 0.4$ and 0.5 (panels A, B, C and D respectively) and different H envelopes (the larger M_{H} , the higher $L_{\text{pp+CNO}}$). The M_{H} values of the sequences shown in the four panels are the same as in Figs 1, 3, 5 and 7, respectively. Note that H-burning luminosity strongly depends upon M_{H} . Note also the sharp increase in the H-burning luminosity for models with very thin H envelopes resulting from the penetration of the H convection zone into the underlying (hotter) He interior.

bute significantly to surface luminosity. For instance, we find that nuclear energy supplies ≈ 55 per cent of the surface luminosity both for the 0.4- M_{\odot} model with $M_{\text{H}}/M=10^{-3}$ and for the 0.3- M_{\odot} model with $M_{\text{H}}/M=2 \times 10^{-3}$, and this contribution is as much as 20 per cent even for the 0.20- M_{\odot} model, but with $M_{\text{H}}/M=4 \times 10^{-3}$. (A detailed discussion of the role played by H burning in carbon–oxygen WDs can be found in, e.g., Iben & Tutukov 1984, Koester & Schönberner 1986 and Mazzitelli & D’Antona 1986.)

Another feature worthy of comment is shown in Fig. 15, in which the evolution of the X_{H} profile for our 0.50- M_{\odot} model with $M_{\text{H}}/M=4 \times 10^{-4}$ is depicted in terms of the fractional mass of the model. The curves correspond to seven different values of T_{eff} , ranging from $\log T_{\text{eff}}=4.51$ to 3.8. The lower panel of Fig. 15 illustrates the behaviour of the energy release due to H burning for the same model and values of T_{eff} as in the upper panel. Note that H burning considerably reduces the value of M_{H} even at quite low T_{eff} . This is also noted for lower stellar masses, but with larger M_{H} values. Apart from ${}^4\text{He}$, the most abundant nucleus produced by H burning is ${}^3\text{He}$ which, for example, eventually reaches an abundance by mass of ≈ 0.043 in the 0.4- M_{\odot} model, with an initial M_{H}/M of 10^{-3} .

Finally, the luminosity of the models versus their ages is illustrated in Figs 16–23. We wish to point out that in such figures we have plotted data *without* taking into account the time elapsed during the binary evolution that leads to the formation of He WDs. Such time is likely to be dependent

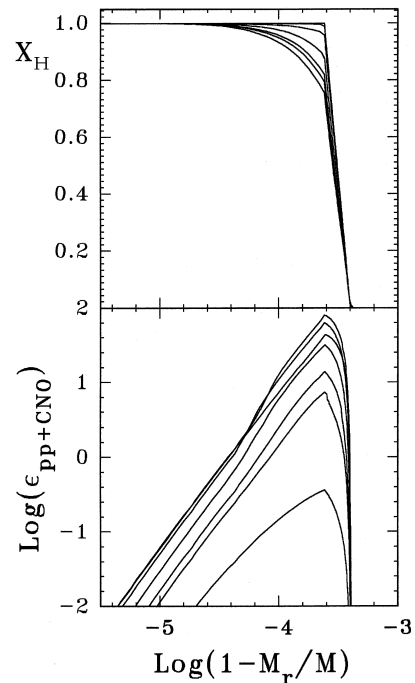


Figure 15. H abundance (upper panel) and energy release (lower panel) due to H burning (in units of $\text{erg s}^{-1} \text{g}^{-1}$) versus the mass fraction for the 0.5- M_{\odot} model with $M_{\text{H}}/M=4 \times 10^{-4}$. In this figure, M_r stands for the mass interior to a sphere of radius r . From top to bottom, the curves correspond to $\log T_{\text{eff}}=4.51, 4.44, 4.30, 4.14, 4.01, 3.96$ and 3.8 (upper panel) and to $\log T_{\text{eff}}=4.44, 4.30, 4.51, 4.14, 4.01, 3.96$ and 3.8 (lower panel). Note the appreciable amount of H burnt during evolution.

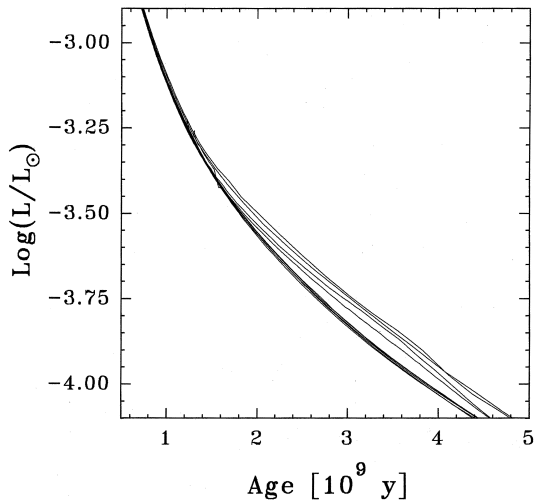


Figure 16. Surface luminosity versus age relation for $0.15\text{-}M_{\odot}$ models with (from top to bottom) $M_{\text{H}}/M=4 \times 10^{-3}$, 2×10^{-3} , 4×10^{-4} , 10^{-3} , 0 , 10^{-8} , 10^{-4} , 10^{-6} and 2×10^{-4} .

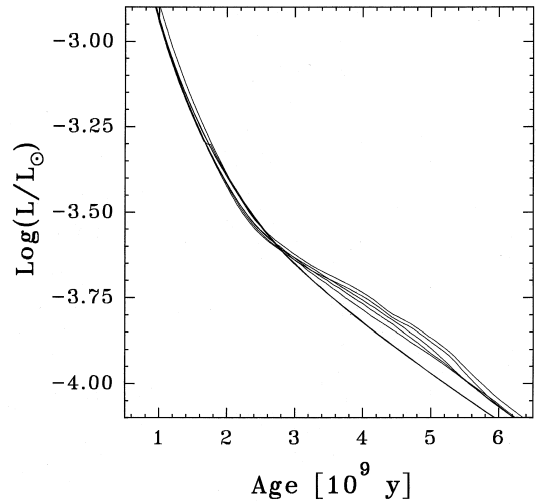


Figure 18. Surface luminosity versus age relation for $0.25\text{-}M_{\odot}$ models. At 4×10^9 yr the curves correspond (from top to bottom) to $M_{\text{H}}/M=2 \times 10^{-3}$, 10^{-3} , 4×10^{-4} , 2×10^{-4} , 10^{-4} , 10^{-6} , 0 and 10^{-8} .

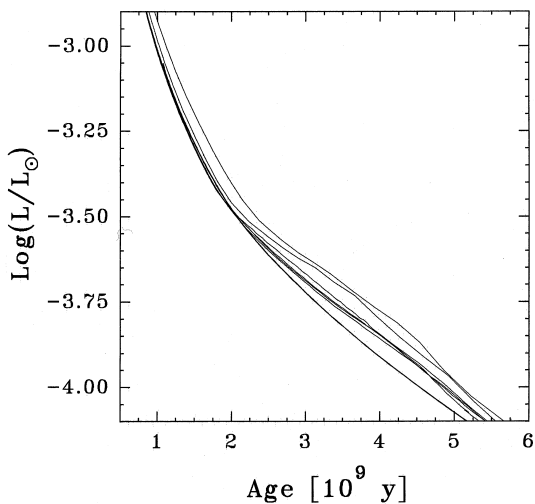


Figure 17. Surface luminosity versus age relation for $0.20\text{-}M_{\odot}$ models. At 3×10^9 yr the curves correspond (from top to bottom) to $M_{\text{H}}/M=4 \times 10^{-3}$, 2×10^{-3} , 10^{-3} , 4×10^{-4} , 10^{-4} , 2×10^{-4} , 10^{-6} , 0 and 10^{-8} .

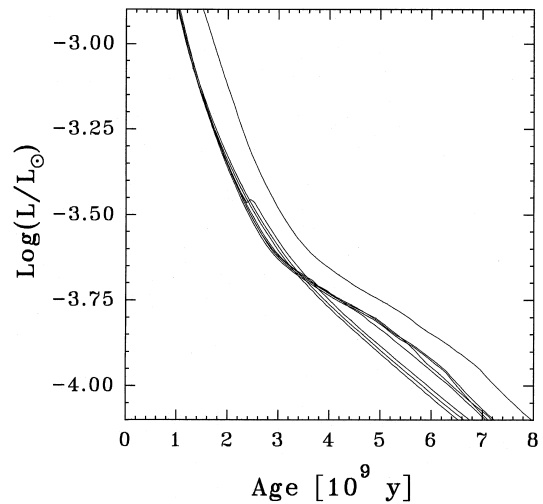


Figure 19. Surface luminosity versus age relation for $0.30\text{-}M_{\odot}$ models with different H envelopes. At 6×10^9 yr the ordering of curves is the same as in Fig. 18. Owing to H burning, the model with $M_{\text{H}}/M=2 \times 10^{-3}$ evolves much more slowly than the other sequences shown in the figure.

on the actual value of M_{H} . If so, the zero age of each sequence of a given mass would not be the same. However, for the range of luminosities considered in the figures, the choice of zero-age point should be of some relevance to the actual stellar age only at the first stages of evolution computed here.

It is worth mentioning that the time spent by models in going through the interval $-2.8 \lesssim \log(L/L_{\odot}) \lesssim -1$ do not depend on M_{H} . This is simply because, at high luminosities, the boundary of the degenerate core is located very deep in the star, which causes the thermal energy content of a given model to be unaffected by possible differences in the outer layer chemical stratification (see Tassoul, Fontaine & Winget 1990 for a discussion in the context of carbon–oxygen WDs). However, for the models with the largest H envelope

that we considered for each stellar mass, some divergences appear. In fact, as stated earlier, the energy release due to H burning is not negligible in such models at intermediate luminosities; thus, they take somewhat longer to evolve to a given luminosity as compared with models with thinner H envelopes. This behaviour is nicely illustrated, particularly in Figs 19 and 21, for instance, which corresponds to the $0.4\text{-}M_{\odot}$ model, we note that, at $\log(L/L_{\odot}) \approx -3$, the age of the sequence with $M_{\text{H}}/M=10^{-3}$ is 35 per cent larger than that corresponding to the case without (or with thinner) H envelope(s). This increases to 50 per cent at $\log(L/L_{\odot}) \approx -2.6$ where, in this particular sequence, the H-burning contribution to the surface luminosity is approximately the same as that resulting from cool-

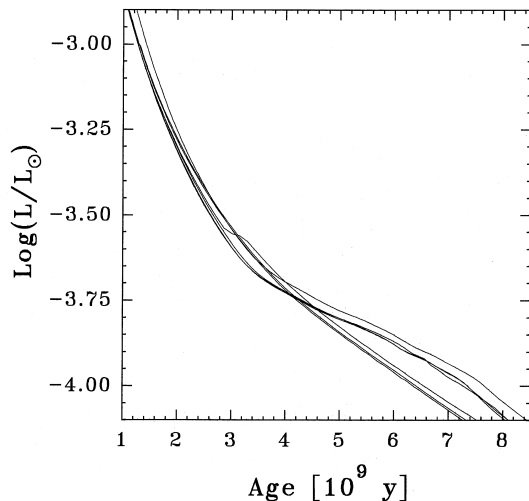


Figure 20. Surface luminosity versus age relation for $0.35\text{-}M_{\odot}$ models. At 6×10^9 yr curves correspond (from top to bottom) to $M_{\text{H}}/M = 10^{-3}$, 10^{-4} , 2×10^{-4} , 4×10^{-4} , 10^{-6} , 10^{-8} and 0.

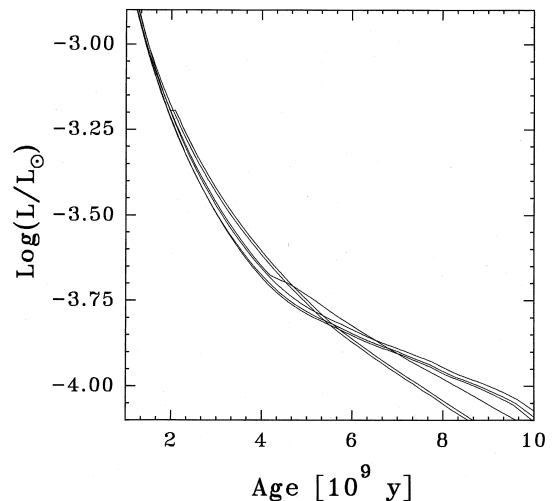


Figure 22. Surface luminosity versus age relation for $0.45\text{-}M_{\odot}$ models. At 4×10^9 yr curves correspond (from top to bottom) to $M_{\text{H}}/M = 10^{-8}$, 0, 10^{-6} , 4×10^{-4} , 2×10^{-4} and 10^{-4} .

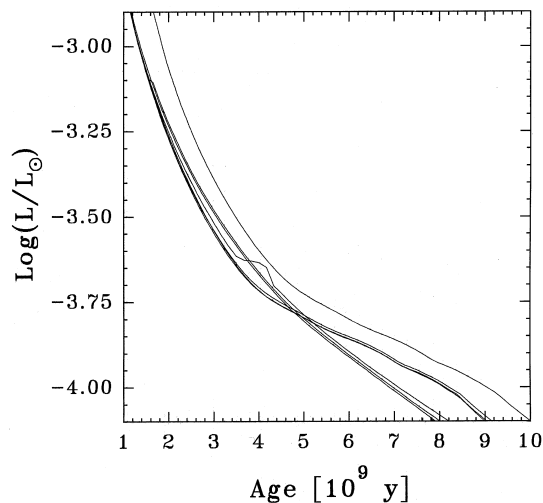


Figure 21. Surface luminosity versus age relation for $0.40\text{-}M_{\odot}$ models. At 7×10^9 yr curves correspond (from top to bottom) to $M_{\text{H}}/M = 10^{-3}$, 4×10^{-4} , 2×10^{-4} , 10^{-4} , 10^{-6} , 10^{-8} and 0.

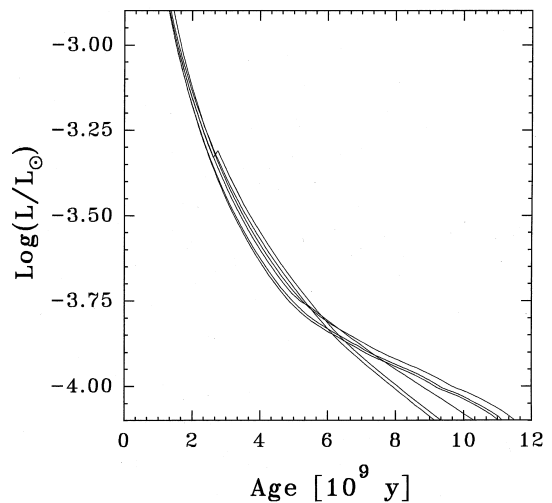


Figure 23. Surface luminosity versus age relation for $0.50\text{-}M_{\odot}$ models. At 4×10^9 yr curves correspond (from top to bottom) to $M_{\text{H}}/M = 10^{-8}$, 0, 4×10^{-4} , 10^{-6} , 2×10^{-4} and 10^{-4} .

ing. Note, also, that the delay in cooling brought about by H burning at intermediate luminosities gives rise to appreciable divergence in the evolutionary times even down to the lowest luminosities shown in these figures.

For $\log(L/L_{\odot}) \lesssim -3$, the cooling curves begin to differentiate appreciably between them. The explanation for this behaviour lies in the fact that, below that luminosity, the central temperature of a model becomes strongly dependent on the presence of an outer H envelope. In this respect, convective mixing may also give rise to substantial changes in the ages of the models. If we concentrate for a moment on examining the age of the $0.5\text{-}M_{\odot}$ model depicted in Fig. 23, we note that in the range $-3.7 \lesssim \log(L/L_{\odot}) \lesssim -2.9$, sequences with thick H envelopes have characteristically shorter ages than those sequences with much

thinner (or no-) H envelopes. This is due simply to the fact that models with thin H envelopes have had to lose a larger fraction of their internal energy as compared with models with thicker H envelopes, with the consequent lengthening of evolutionary times during this phase of evolution. Note, however, that in the range $-3.8 \lesssim \log(L/L_{\odot}) \lesssim -3.3$, the model with $M_{\text{H}}/M = 10^{-8}$ takes longer to evolve than any other sequence as a result of the sharp change of the outer layer composition brought about by convective mixing. This last phenomenon is also visible in the 0.35- and $0.40\text{-}M_{\odot}$ models with $M_{\text{H}}/M = 10^{-6}$, as shown by Figs 20 [at $\log(L/L_{\odot}) \approx -3.55$] and 21 [at $\log(L/L_{\odot}) \approx -3.62$], respectively. Eventually, when convection reaches the degenerate core in models with very thick H envelopes, their central temperature drops markedly, thus reversing the trend in the evolu-

tionary times noted previously. These results qualitatively agree with those of D'Antona & Mazzitelli (1989) and Tasouli et al. (1990) for the case of carbon–oxygen WDs.

Because less massive models are less degenerate and thus a greater fraction of their mass is convective, their cooling curves behave somewhat differently. In fact, we note from Table 1 that, for instance, the 0.15- M_{\odot} models require $M_{\text{H}}/M \gtrsim 4 \times 10^{-4}$ to retain an appreciable amount of H after mixing episodes. When convection penetrates into the degenerate core of such models, their central temperatures will be accordingly much lower as compared with models with thinner H envelopes, thus implying longer evolutionary times, as illustrated in Fig. 16.

4 DISCUSSION AND CONCLUSIONS

In this paper we computed low- and intermediate-mass helium white dwarf (He WD) models with masses from $M = 0.15$ to $0.5 M_{\odot}$ and different hydrogen (H) envelope mass fractions. We treated the mass of the H envelope (M_{H}) as essentially a free parameter within the range $10^{-8} \leq M_{\text{H}}/M \leq 4 \times 10^{-3}$. In addition, we computed the evolution of models with no-H envelopes for the same masses. These models were evolved from the hot WD stage down to $\log(L/L_{\odot}) = -5$.

The calculations were carried out by using a detailed WD evolutionary code in which we included updated radiative opacities and equations of state for H and He plasmas; the effects of convective mixing and hydrogen burning (proton–proton chain and CNO bi-cycle) were also fully taken into account. In particular, the energy transport by convection was described by the self-consistent model for stellar turbulent convection recently developed by Canuto et al. (1996), which represents a substantial improvement with respect to older convection models.

Since our models are constructed by employing the best input physics available at present, we believe that the results obtained in this study together with those presented in Paper I represent the most comprehensive study of the structure and evolution of realistic models of low- and intermediate-mass He WDs to date.

The emphasis of this paper was focused on the effects on the structure of He WD models by varying the mass of the H envelope. In this context, we found that thick H envelopes appreciably modify the radii and surface gravities of the no-H models, especially in the case of low-mass configurations. We also found that convective mixing in models with very thin H envelopes eventually turns such models into objects with He-dominated outer layers. In addition, the role played by H burning in these stars is strongly dependent on M_{H} .

Finally, the effect of H envelopes on the evolutionary times was also investigated. In this respect, we found that, apart from models for which H burning contributes substantially to the surface luminosity, the cooling times in the interval $-2.8 \lesssim \log(L/L_{\odot}) \lesssim -1$ do not depend upon M_{H} . In contrast, this behaviour is not verified at lower luminosities, where appreciable differences in the evolutionary times arise.

It is an usual technique to measure the mass of a WD by applying the surface gravity–effective temperature relation. It is obvious from our results that in the domain of low-mass

He WDs, there exists a very important and (perhaps) unavoidable source of uncertainty arising from the impossibility of measuring the actual mass fraction of H present in WD. This uncertainty is especially dramatic in low-mass objects: note that in Fig. 9, at $T_{\text{eff}} \approx 10\,000$ K, the surface gravity of a 0.15- M_{\odot} He WD with no H is almost coincident with that of the object of 0.20- M_{\odot} with $M_{\text{H}}/M = 4 \times 10^{-4}$. This fact imposes upper limits on the precision of the measurements we can make by employing this technique. The implications of the existence of such upper limits on the determination of the characteristics of the WD itself, and of the companion objects in binary systems, like those studied by van Kerkwijk et al. (1996), surely deserve further attention.

We postpone, to a later publication, the application of the evolutionary results presented in this paper to interpretation of recent observations of low-mass white dwarfs. Detailed tabulations of the evolution of our low- and intermediate-mass He WD models, which are not reproduced here, are available upon request to the authors at their e-mail addresses.

ACKNOWLEDGMENTS

We warmly thank Paul Bradley for suggesting that we perform this study. This work has been partially supported by the Comisión de Investigaciones Científicas de la provincia de Buenos Aires, the Consejo Nacional de Investigaciones Científicas y Técnicas (Argentina) through the Programa de Fotometría y Estructura Galáctica (PROFOEG), and the University of La Plata.

REFERENCES

- Alexander D. R., Ferguson J. W., 1994, *ApJ*, 437, 879
- Althaus L. G., Benvenuto O. G., 1996, *MNRAS*, 278, 981
- Althaus L. G., Benvenuto O. G., 1997a, *ApJ*, 477, 313 (Paper I)
- Althaus L. G., Benvenuto O. G., 1997b, *MNRAS*, 288, L35
- Althaus L. G., Benvenuto O. G., 1997c, *MNRAS*, submitted
- Arnett W. D., Truran J. W., 1969, *ApJ*, 157, 339
- Benvenuto O. G., Althaus L. G., 1995, *Ap&SS*, 234, 11
- Benvenuto O. G., Althaus L. G., 1997, *MNRAS*, 288, 1004
- Canuto V. M., Mazzitelli I., 1991, *ApJ*, 370, 295 (CM)
- Canuto V. M., Mazzitelli I., 1991, *ApJ*, 389, 724 (CM)
- Canuto V. M., Goldman I., Mazzitelli I., 1996, *ApJ*, 473, 550 (CGM)
- Caughlan G. R., Fowler W. A., 1988, *Atomic Data and Nuclear Data Tables*, 40, 290
- Cox A. N., Stewart J., 1970, *ApJS*, 19, 261
- D'Antona F., Mazzitelli I., 1979, *A&A*, 74, 161
- D'Antona F., Mazzitelli I., 1989, *ApJ*, 347, 934
- Iben I., Jr, Livio M., 1993, *PASP*, 105, 1373
- Iben I., Jr, McDonald J., 1985, *ApJ*, 296, 540
- Iben I., Jr, Tutukov A. V., 1984, *ApJ*, 282, 615
- Iben I., Jr, Tutukov A. V., Yungelson L. R., 1996, *ApJ*, 475, 291
- Iglesias C. A., Rogers F. J., 1993, *ApJ*, 412, 752
- Koester D., Schönberner D., 1986, *A&A*, 154, 125
- Landsman W., Aparicio J., Bergeron P., Di Stefano R., Stecher T. P., 1997, *ApJ*, 481, L93
- Lundgren S. C., Cordes J. M., Foster R. S., Wolszczan A., Camilo F., 1996, *ApJ*, 458, L33
- Marsh T. R., 1995, *MNRAS*, 275, L1
- Marsh T. R., Duck S. R., 1996, *MNRAS*, 278, 565

- Marsh T. R., Dhillon V. S., Duck S. R., 1995, MNRAS, 275, 828
Mazzitelli I., D'Antona F., 1986, ApJ, 308, 706
Moran C., Marsh T. R., Bragaglia A., 1997, MNRAS, 288, 538
Provencal J. L., Shipman H. L., Thejll P., Vennes S., Bradley P. A.,
1996, ApJ, 466, 1011
Rogers F. J., Iglesias C. A., 1994, Sci, 263, 50
- Saumon D., Chabrier G., Van Horn H. M., 1995, ApJS, 99, 713
Tassoul M., Fontaine G., Winget D. E., 1990, ApJS, 72, 335
van Kerkwijk M. H., Bergeron P., Kulkarni S. R., 1996, ApJ, 467,
L89
Wagoner R. V., 1969, ApJS, 18, 247
Wallace R. K., Woosley S. E., Weaver T. A., 1982, ApJ, 258, 696